

Optimization of Steam Ejector Performance Using CFD

Tarek A. Ghonim^{*}, Ahmed S. Hegazy, and Mohamed S. Farag

Mechanical Power Eng. Department, Faculty of Eng., Menoufia University, Shebin El-Kom, Egypt.

**Corresponding author: tarek_ghonim@sh-eng.menofia.edu.eg*

ABSTRACT

The present work introduces a numerical investigation of steam ejector optimum performance at constant pressure ratio used in many applications. The present study aims to maximize the ejector efficiency by optimizing the ejector mass ratio. The effect of geometrical parameters on ejector mass ratio and its efficiency is investigated at constant operating conditions. These parameters are the ejector convergent section angle, the constant area mixing chamber length and the angle of the ejector divergent section. The results showed that the ejector wall static pressure distributions were greatly affected by the investigated geometrical parameters. Furthermore, In order to avoid separation, the ejector divergent section angle must be selected carefully together with the operating conditions. The ejector mass ratio and efficiency increased with increasing the previously stated three geometrical parameters to gain their upper limit values, subsequent to that, the efficiency and mass ratio decreased with increasing these geometrical parameters indicating that there are optimum geometrical parameters. Moreover, an optimum value of the ejector efficiency and mass ratio took place at about $\beta = 4.8^\circ$, $L_{CA} = 70$ mm and $\alpha = 3.6^\circ$ at given operating conditions.

Keywords: *Steam Ejector, CFD, Maximum Mass Ratio, Optimum Geometry, Ejector Efficiency*

1. Introduction

Ejectors are frequently encountered in many different applications such as refrigeration systems due to low energy consumption and reliability. Another important application is the multi-effect distillation (MED) that reduces the consumption of energy of seawater desalination systems greatly when used in combination with thermal vapor compression (TVC) fulfilled through using steam ejector. The optimization of steam ejector performance can improve the energy efficiency of MED-TVC desalination systems. Ejectors are generally used due to their easy construction and simple operation. However, ejector operation involves severe irreversible mixing and friction resulting in a very low thermodynamic efficiency. A highly pressurized motive steam in the ejector is known as the primary fluid. The primary fluid flows through a motive flow nozzle to entrain the secondary fluid. The primary and secondary flows mix together in a duct and then the flow pressure is recovered in a diffuser. Theoretically, there must be a complete swap of momentum at the end of mixing duct producing a uniform mixed stream flow travelling at a mean velocity between the motive and suction flow velocities. A diffuser is fitted in order to reduce the losses as possible by decreasing gradually the flow

velocity to convert the exit kinetic energy from the mixing duct to pressure.

Numerous early experimental and theoretical studies focused on the enhancement of ejector efficiency to overcome the low COP of the ejector based systems to be more economically attractive. A steam ejector refrigerator designed for operation at high evaporator and boiler temperatures and low temperature of the condenser should have higher COP and should need larger area ratio ejector than otherwise [1]. Optimal performance of fixed-geometry ejectors for refrigeration systems is difficult to achieve under various operating conditions [2]. As increasing both the boiler and evaporator temperatures would require decreasing the ejector geometry whilst increasing the condenser temperature would require decreasing it. A parametric simulation study on steam injector performance indicated that the throat diameter of the mixing section, the central liquid conduit position, and area contraction ratio were responsible for the steam injector functioning range [3]. For high area contraction ratios, high discharge pressures could be attained however the working range decreased. Riffat and Omer [4] studied the effect of the exit position of the nozzle (NXP) on the ejector performance and showed that a better performance will be obtained with locating the nozzle exit at least 0.21 length of

the throat diameter of the mixing chamber upstream of the mixing chamber entrance than pushing it into the mixing chamber. Aphornratana and Eames [5] studied experimentally the effect of the NXP on the COP of a steam-ejector refrigerator. The results indicated that the cooling capacity and COP could be changed as much as 100% by changing the NXP. Which is confirmed experimentally, through the pressure profile analysis along a steam-ejector refrigerator given by [6]. Not only the NXP was found effective, but the nozzle size as well.

Through the past decades, computational fluid dynamics (CFD) methods have been regarded as an efficient means to analyze ejector performance and to predict its behavior. The nozzle exit position (NXP) and the constant-area mixing section diameter were shown to be important ejector design parameter. However, the constant-area diameter improved the ejector performance only when operating in critical mode with a shock in the diffuser [7]. Two ejector optimization techniques using and constant-pressure ejector flow models were presented and compared by Yapici and Ersoy [8]. The results showed that the optimum area ratio determined using constant-area model was greater than that of the constant-pressure one. The optimum area ratio increased with generator temperature, decreased with condenser temperature and was much less affected by the variation in evaporator temperature. CFD investigation on the characteristics and efficient design of an ejector used in refrigeration systems showed that the suction zone shape has not affected the performance of the ejector as the flow patterns of axisymmetric and 3D simulation were similar [9].

Hewedy et al. [10] presented a comprehensive optimization of air ejectors at different and wide ranges of operating conditions and geometries. However, that previous work did not consider the change in both convergent and divergent angles of the ejector mixing duct and diffuser. Different optimum design correlations were deduced at given ejector angles to maximize the ejector efficiency and it was concluded that the entire optimization would change negatively if the ejector angles changed. Two kinds of mixing chamber structure including the convergent and constant-area sections were proposed to enhance ejector performance, one is for optimum entrainment ratio, and the other is for optimum critical discharging pressure [11]. Performance prediction of steam ejector for refrigeration applications using CFD was studied by Sriveerakul et al. [12, 13]. The ejector optimum performance was investigated and found to be mainly governed by both operating conditions and geometries. The complications of the flow and the mixing process in the ejector such as phenomena on choked flow, jet

core effect and presence of oblique shocks were discussed. It was shown that the effective area does exist; however, it was difficult to locate its exact position within the ejector conduit. Additionally, both entrainment ratio and critical back pressure could be varied simultaneously by adjusting three parameters, namely the primary fluid saturated pressure, the secondary fluid saturated pressure and the primary nozzle size. Furthermore, the area ratio between the nozzle and constant-area section, NXP and constant-area section length influenced considerably both entrainment ratio and critical back pressure. Obviously, an optimal area ratio existed depending on the ejector operating conditions [14].

Varga et al. [15] investigated numerically ejector efficiencies of the primary nozzle, suction, mixing and diffuser sections at different nozzle diameters. The results indicated the nozzle efficiency was only slightly affected by nozzle diameter. The efficiencies for the mixing process increased slightly with back pressure until an optimum value beyond which they considerably dropped while the diffuser efficiency depended on the condenser conditions. The operating and structural parameters including the length of mixing chamber, length of the second throat, diameter of the second throat and diameter of the primary nozzle were found effective in optimum design of steam ejector [16]. Where, optimal values of these parameters are needed for maximizing the entrainment ratio. Moreover, the optimum geometries of two-phase flow ejector for refrigeration applications were correlated to the operating conditions by Ghonim [17]. It was stated that the maximum ejector efficiency is mainly dependent on the correct choice of the geometries which suits the operating conditions range.

More recently, Wang et al. [18] performed a systematic investigation on an ejector refrigeration system operating near the critical back pressure. The primary pressure was varied to achieve the highest efficiency through obtaining an optimum entrainment ratio at critical back pressure. Huang et al. [19] Simulated and optimized a new ejector refrigeration system under different ambient temperatures. It was concluded that the compressor work of the optimized ejector could be reduced by 10% resulting in an increase in COP of 11% at ambient temperature of 35° C. Chen et al. [20] presented a model for evaluation of the ejector nozzles performance used in refrigeration systems. It is clarified that the predicted ejector nozzles performance based on an ideal gas assumptions can be significantly different from that based on the real fluid properties. Because for the two-phase nozzle, the speed of sound error value may cause huge differences in the performance of the nozzle and even predictions of the efficiency of

nozzle are greater than unity. Zhang et al. [21, 22] used ideal gas assumption CFD model to investigate the effect of friction losses on the efficiency of ejector, and showed that it diminished 12.9% when roughness increased from 5μ to 100μ. The ejector is composed of five categories: a suction chamber, nozzle, constant-area section, mixing chamber, and diffuser. It was also pointed out that the diffuser and the constant-area sections have the most effective impact on performance of an ejector. When the diffuser and constant-area surface roughness increased from 5μ to 300μ, the entrainment ratio was decreased by 12.15% and 8.7%, respectively.

Hence, as has been discussed previously, the performance of an ejector is very sensitive to its geometry and a little change in it can affect greatly and negatively the ejector performance. Although there were numerous researches on the ejector geometries, no enough information was found in the available massive literature on estimating the optimum geometries which can attain the ideal flow pattern resulting in minimum fluid energy dissipation. Therefore, the ultimate motivation behind the present work is to optimize the steam ejector performance (efficiency) by maximizing the mass flow ratio by selecting the optimum geometries at constant operating pressures. This will be fulfilled through the following:

- 1) Development and validation of a 2-D mathematical model to predict the suction mass flow rate of supersonic steam ejectors,
- 2) Selecting the optimum angles of the convergent mixing duct and the diffuser of an ejector in order to optimize the mass ratio for a given operating pressures,
- 3) Selecting the optimum constant area mixing duct length of an ejector to optimize the mass ratio for the same operating pressures as well, and
- 4) Relating the ejector mass ratio and efficiency to the investigated ejector geometrical parameters by numerically based correlations deduced from the theoretical investigation to optimize the ejector design (maximum efficiency).

2. Mathematical Model

The governing equations that describe the behavior of flow through ejectors are presented in this section. The theoretical model is formulated using these assumptions: single-phase flow, two-dimensional, turbulent and compressible flow. A horizontal ejector is considered and the flow is steady axisymmetric. The working fluid of the proposed model (water vapor) is considered an ideal gas. Although the single-phase ideal gas assumption seems to be unrealistic, it was reported by some researchers [12,

13 & 23], that similar results to a real gas model were obtained when the operating pressures are relatively low. The properties of water vapor given in the database of FLUENT are listed in Table 1. The working fluid density is calculated using the ideal gas relation and other properties are defined as constants throughout the simulation. The governing equations are written as in [23, 24 & 25]:

The equation of mass conservation is

$$\frac{\partial}{\partial x}(\rho u) + \frac{\partial}{\partial r}(\rho v) + \frac{\rho v}{r} = 0 \quad (1)$$

The equations for momentum conservation are

$$\frac{\partial}{\partial x}(\rho uu) + \frac{1}{r} \frac{\partial}{\partial r}(r \rho uv) = \frac{\partial}{\partial x} \left[\mu_{eff} \left(2 \frac{\partial u}{\partial x} - \frac{2}{3} (\nabla \cdot \vec{u}) \right) \right] - \frac{\partial p}{\partial x} + \frac{1}{r} \frac{\partial}{\partial r} \left[r \mu_{eff} \left(\frac{\partial u}{\partial r} + \frac{\partial v}{\partial x} \right) \right] + \rho g + S_u \quad (2)$$

$$\frac{\partial}{\partial x}(\rho uv) + \frac{1}{r} \frac{\partial}{\partial r}(r \rho vv) = -\frac{\partial p}{\partial r} + \frac{\partial}{\partial x} \left[\mu_{eff} \left(\frac{\partial u}{\partial r} + \frac{\partial v}{\partial x} \right) \right] + \frac{1}{r} \frac{\partial}{\partial r} \left[r \mu_{eff} \left(2 \frac{\partial v}{\partial x} - \frac{2}{3} (\nabla \cdot \vec{u}) \right) \right] - 2 \mu_{eff} \frac{v}{r^2} + \frac{2}{3} \frac{\mu_{eff}}{r} (\nabla \cdot \vec{u}) + S_v \quad (3)$$

The source terms for momentum in x and r directions are S_u and S_v respectively, and

$$\nabla \cdot \vec{u} = \left(\frac{\partial u}{\partial x} + \frac{\partial v}{\partial r} + \frac{v}{r} \right)$$

The conservation equation of energy in steady 2-D (x-r) coordinate system is

$$\frac{\partial}{\partial x} [u(\rho E + p)] + \frac{1}{r} \frac{\partial}{\partial r} [rv(\rho E + p)] = \frac{\partial}{\partial x} \left[\lambda_{eff} \left(\frac{\partial T}{\partial x} - \sum h_i J_{ix} \right) + \left(\vec{\tau}_{eff} \cdot \vec{V} \right)_x \right] + \frac{1}{r} \left[r \lambda_{eff} \frac{\partial T}{\partial x} (\sum h_i J_{ir} +) + \left(\vec{\tau}_{eff} \cdot \vec{V} \right)_r \right] + S_h \quad (4)$$

Where, $\vec{\tau}_{eff}$ is the turbulent shear stress tensor, \vec{V} is the velocity vector and S_h is the energy source term.

The efficiency of steam ejector is given by [25].

$$\eta = MR \frac{h_b - h_s}{h_m - h_b} \quad (5)$$

Where, h_b , h_s and h_m are the enthalpies of the back, suction and motive steams, respectively which are

obtained from REFPROP, as reported by [20] at constant pressure and temperature. MR is the mass ratio (ratio of suction to motive mass flow rates).

Table 1. Working fluid properties (water vapor) [24]

Property	Value
Viscosity, μ	1.34×10^{-5} kg/m. s
Thermal conductivity, K	0.02610 W/m. K
Specific heat capacity, Cp	2014.0 J/kg. K
Molecular weight, Mw	18.0153 kg/ kmol

3. Turbulence modeling

The turbulence model adapted in this work is the realizable k- ϵ model [23, 24, and 26]. Additionally, this model provides a better performance in case of rotational flow, severe adverse pressure gradient boundary layer and separated flow which is possibly encountered in diffusers of steam ejectors [13, 23, and 24]. The standard and realizable k- ϵ models differ in two crucial things. The realizable one has a new for the turbulent viscosity formulation. Moreover, it derived a new equation for the dissipation rate transport, ϵ using an exact equation for the transport of the mean-square vorticity fluctuation.

The turbulent kinetic energy and the rate of dissipation are given by [18]:

$$\frac{\partial}{\partial x}(\rho uk) + \frac{1}{r} \frac{\partial}{\partial r}(r \rho vk) = \frac{\partial}{\partial x} \left[\left(\mu + \frac{\mu_t}{\sigma_k} \right) \frac{\partial k}{\partial x} \right] + \frac{1}{r} \frac{\partial}{\partial r} \left[r \left(\mu + \frac{\mu_t}{\sigma_k} \right) \frac{\partial k}{\partial r} \right] + G_k + G_b - \rho \epsilon + S_k \quad (6)$$

$$\frac{\partial}{\partial x}(\rho u \epsilon) + \frac{1}{r} \frac{\partial}{\partial r}(r \rho v \epsilon) = \frac{\partial}{\partial x} \left[\left(\mu + \frac{\mu_t}{\sigma_\epsilon} \right) \frac{\partial \epsilon}{\partial x} \right] + \frac{1}{r} \frac{\partial}{\partial r} \left[r \left(\mu + \frac{\mu_t}{\sigma_\epsilon} \right) \frac{\partial \epsilon}{\partial r} \right] + \rho C_1 S_\epsilon - \rho C_2 \frac{\epsilon^2}{k + \sqrt{\nu \epsilon}} + C_{1\epsilon} \frac{\epsilon}{k} C_{2\epsilon} G_b - S_\epsilon \quad (7)$$

Where, G_k is the turbulent kinetic energy generation caused by the gradients of mean velocity and G_b represents the turbulence kinetic energy generation caused by buoyancy. The fluctuating dilatation contribution in the compressible turbulence to the overall rate of dissipation is neglected. The user-defined source terms are S_k and S_ϵ . Where,

$$C_1 = \max \left[0.43 \frac{\eta^*}{\eta^* + 5} \right], \eta^* = S \frac{k}{\epsilon}, S = \sqrt{2 S_{ij} S_{ij}} \quad (8)$$

The strain rate tensor (S_{ij}), the notation (ij) describes the direction. When i or $j = 1$, this case

corresponding to the x -direction, i or $j = 2$ means the r -direction.

In turbulence modeling,

$$\mu_t = \rho C_\mu \frac{k^2}{\epsilon}, \mu_{eff} = \mu + \mu_t$$

4. Procedure of solution

The numerical solution is obtained using FLUENT 6.3 with finite volume solver, [24]. Where an axisymmetric compressible two-dimensional Reynolds averaged Navier-Stokes (RANS) equations with the realizable k- ϵ turbulence model are adapted.

The steam ejector considered in the present study is constructed of an ejector and a primary flow nozzle. A secondary flow is sucked by the ejector due to strong acceleration of the primary flow in the nozzle. The physical domain, boundary conditions, the computational domain and the main geometrical parts are the mixing chamber, secondary inflow, diffuser and throat as illustrated in Fig.1.

The segregated solver is used for solving the discretization equations with the boundary and initial conditions. The momentum and mass conservations are sequentially solved with an equation of pressure correction. The computational mesh generated for simulating steam ejector corresponds to the measurements of [12, 13]. The effect of grid refinement on the quality of results is tested in the present study of steam ejector, in which 6200 nodes for the first nozzle part and 16950 nodes for the second mixture part. For ideal steam flow, the properties of saturated steam (pressure and temperature), are used in the inlet flow. The boundary condition at exit is pressure outlet. Since the flow is axisymmetric about the ejector center line, only the upper half is considered for the CFD computations

5. Results and discussion

The ejector performance is mainly characterized by mass ratio and the ejector efficiency. A well designed steam ejector is the one that can deliver the maximum attainable mass ratio with higher efficiency.

Figure 2 presents the code validation based on the experimental data provided by Sriveerakul et al. [12, 13]. It is clearly shown that the presented code is capable of predicting the ejector performance well. In addition, Fig. (2.a) shows that the mass ratio is constant with back pressure increment until a certain value which is called the breakdown point. By increasing the back pressure higher than the breakdown point a reversed flow region dominated at the ejector exit. Which results in delivering the steam flow back to the suction inlet and the ejector dramatically malfunctions.

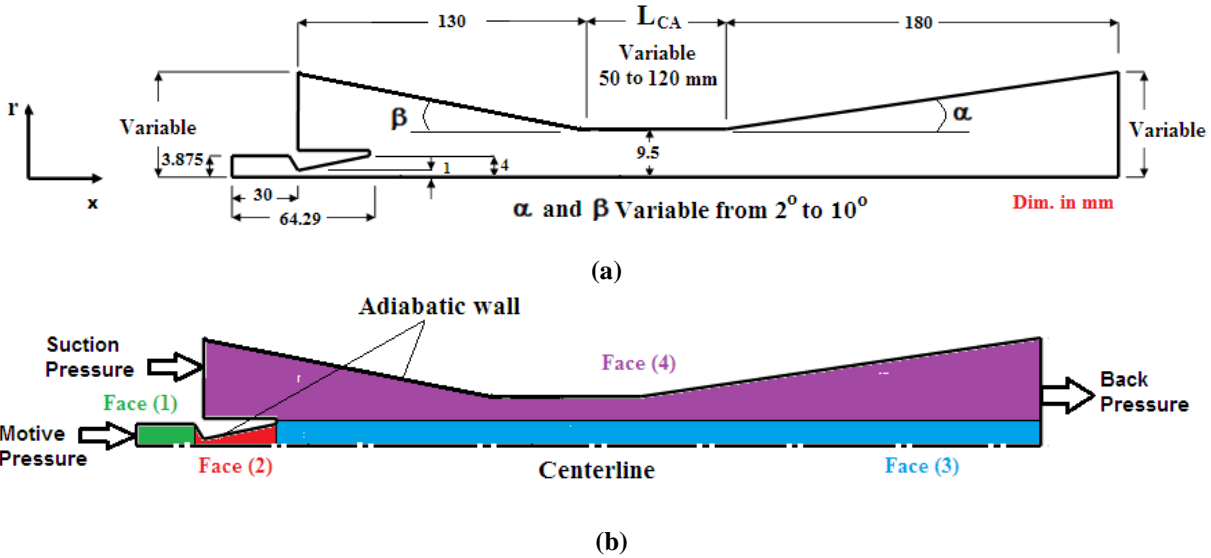


Fig. (1)- (a) Schematic drawing of the physical domain, (b) boundary conditions and the computational domain for the steam ejector

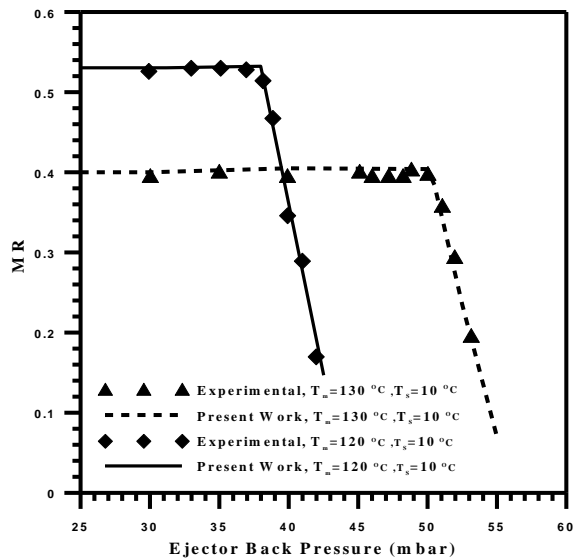


Fig. (2. a) Effect of back pressure on mass ratio of steam ejector based on experimental data provided by Sriveerakul et al. [12]

However, Fig. (2.b) illustrates that present numerically predicted static pressure profile along the ejector was compared well to the experimental data provided by [12]. The maximum absolute prediction errors of mass ratio and static pressure were found to be about 3.57% and 4.13%, respectively. Fig. (2.c and d) depict Mach number contours compared to

numerical results of Sriveerakul et al. [13] and present numerical Mach number and static pressure distributions along the ejector showing shocking position at A-A respectively. However, the fluctuations in both pressure and Mach number, shown in Fig. (2.d), are apparently due to an incomplete mixing of motive and suction flows.

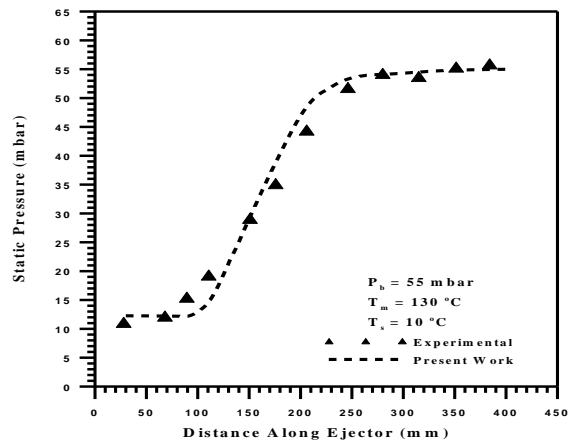


Fig. (2. b) Comparison between present numerical static pressure profile along the ejector and experimental data provided by Sriveerakul et al. [12]

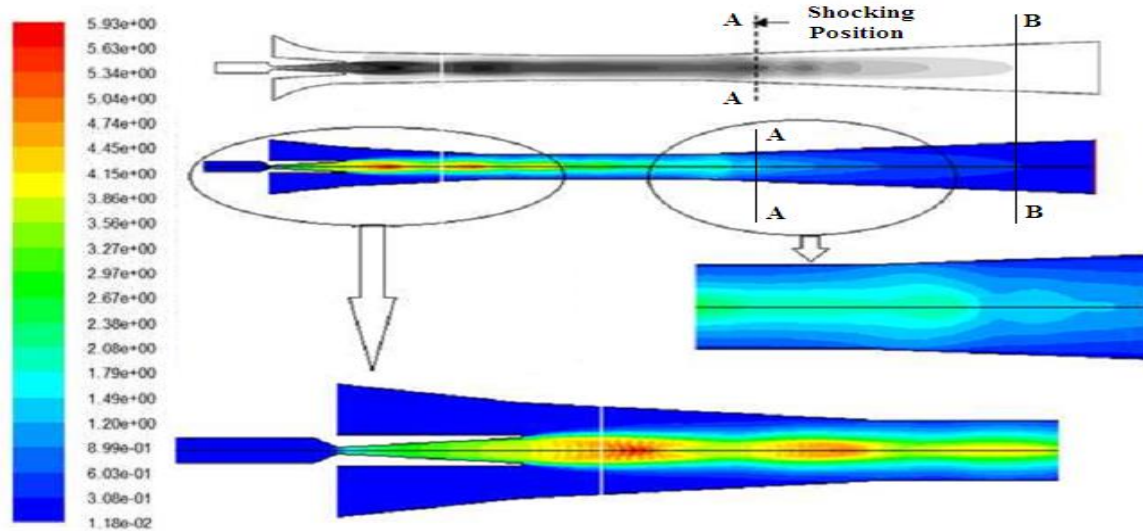


Fig. (2. c) Comparison of the present numerical Mach number contours with the numerical results of Sriveerakul et al. [13] at $P_b = 30$ mbar, $T_m = 130$ °C and $T_s = 10$ °C

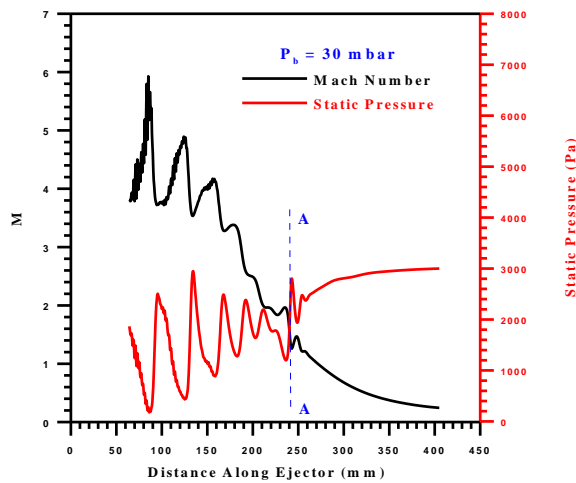


Fig. (2. d) Present numerical Mach number and static pressure distributions along the ejector showing shocking position at A-A given in Fig. (2. c)

The steam ejector efficiency given in Eqn. (5) can be enhanced by optimizing the ejector mass ratio, MR and its operating pressures as well (motive (P_m), suction (P_s) and back (P_b) pressures). M. S. Farag, [25] enhanced the ejector efficiency up to 55% by operating it at low pressure ratios for a given ejector geometry. However, present results concern with enhancing the steam ejector efficiency by optimizing its mass ratio at different ejector geometries. A motive flow nozzle with throat radius of 1 mm and an exit radius of 4 mm was used in the numerical simulation. In addition, the constant-pressure mixing section length, the constant-area mixing section

radius and the diffuser length were 130, 9.5, and 180 mm, respectively. While, the operating pressures P_m , P_s and P_b were given constant values of 2.7, 0.06, and 0.075 bar respectively as well.

The effect of the constant-pressure mixing section half angle, β on the wall static pressure distribution along the ejector axis is shown in Fig. (3. a). It can be observed clearly in the figure that increasing the constant-pressure mixing section half angle leads to an increase in the static pressure along the ejector mixing sections. No abrupt pressure rise is seen in the diffuser section as a pressure outlet boundary condition is set at the exit. The increase in the static pressure at the ejector inlet may be attributed to the increase in the secondary flow suction area due to increasing the constant-pressure mixing section angle while keeping its length and exit diameter constants. Increasing the secondary flow suction area will consequently decrease the flow velocity and increase its pressure. For a given constant-pressure mixing section half angle, the pressure is decreased up to the exit of the constant-pressure mixing section. This decrease in pressure is due to the decrease of the flow area along the ejector axis and friction as well which dominated the tendency for pressure rise caused by the mixing process itself. Furthermore, in the constant-area mixing section the static pressure increases up to a certain distance and decreases after it for almost all values of the angles, β . The increase in the pressure may be explained by the mixing process which is still taking place. However, after completion of the mixing process, the static pressure decreases only due to friction. Figure (3. b) illustrates the effect of the constant-pressure mixing section half angle, β on the centerline Mach number distribution

along the ejector axis. The fluctuation of Mach number is apparently due to incomplete mixing of both flows. No effect of the angle β is surely noticed along the axis of the primary flow supersonic nozzle and a very slight effect is seen in the constant-pressure mixing section. This is apparently because the mixing process is still at the beginning which means that only primary flow exits in the flow core. Moreover, after the onset of the mixing process in the constant-area mixing section it is seen that the effect of the angle β is opposite to that in Fig. (3, a). Increasing the flow Mach number will lead to an increase in the flow velocity and a decrease in its pressure.

The ejector mass ratio, MR and consequently its efficiency are greatly affected by constant-pressure mixing section half angle, β which is depicted in Fig. 4. An optimum value of the mass ratio took place at about $\beta = 4.8^\circ$ leading to a maximum efficiency of about 10.8. Furthermore, the influences of the constant-area mixing section length, L_{CA} on both wall static pressure and Mach number distributions along the ejector axis are illustrated respectively in Fig. 5. Generally, decreasing the constant-area mixing section length caused the static pressure to increase due to less friction except for $L_{CA} = 50$ mm.

This is apparently because for $L_{CA} = 50$ mm the constant-area mixing section length was not long enough to complete mixing of the primary and secondary flows. Figure 6 depicts the effect of the constant-area mixing section length on both ejector efficiency and mass ratio. Both maximum efficiency and mass ratio took place at $L_{CA} = 70$ mm.

On the other hand, the effect of diffuser section half angle, α on the wall static pressure distribution along the ejector axis is shown in Fig. (7. a). It is shown clearly that increasing the diffuser half angle, α leads to an increase in the static pressure along the ejector axis due to an increase in the flow area except at the exit which is set as a boundary condition. Almost an opposite effect of the diffuser angle on the centerline Mach number distribution along the ejector length is reasonably shown in Fig. (7. b). The mass ratio is apparently affected by the diffuser angle which is depicted in Fig. 8. An optimum value of the mass ratio took place at about 3.6° of the diffuser half angle. It is important to determine the optimum angle of the diffuser at a given operating condition for optimum efficiency of the ejector. Otherwise, the unoptimized diffuser angle will consequently lead to a diminished value of both ejector efficiency and mass ratio.

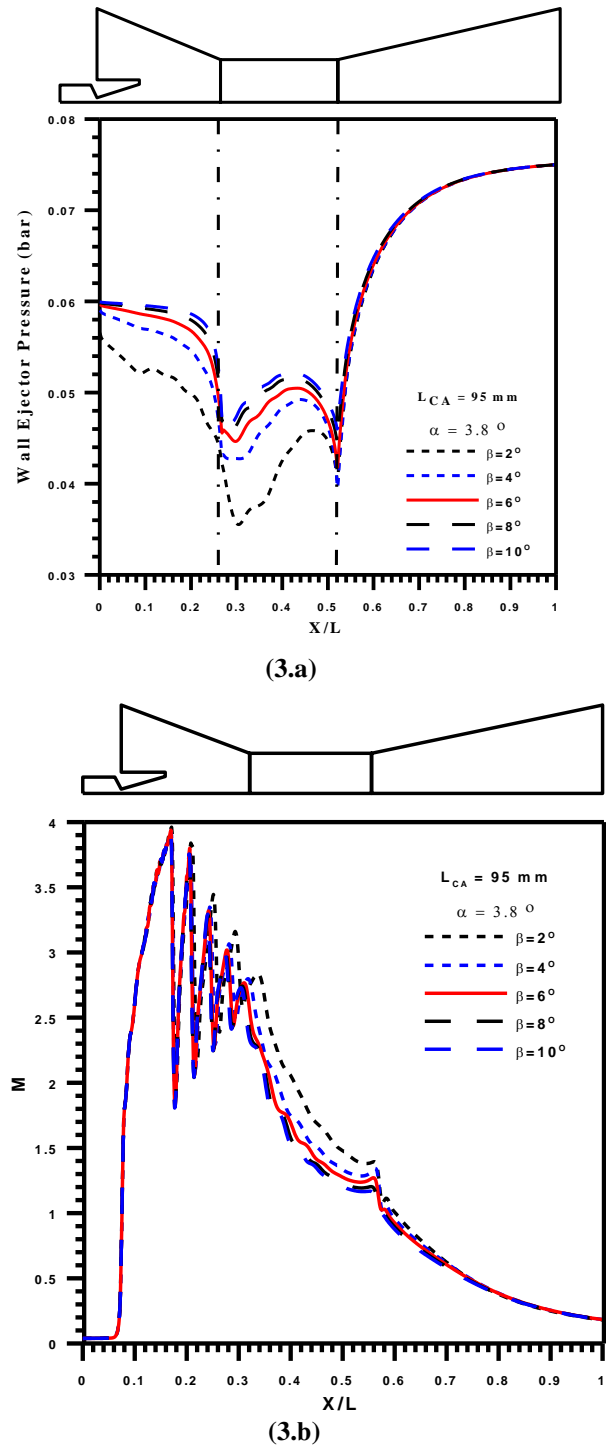


Fig. 3 Effect of constant-pressure mixing section half angle on wall static pressure and centerline Mach number distributions along the ejector axis.

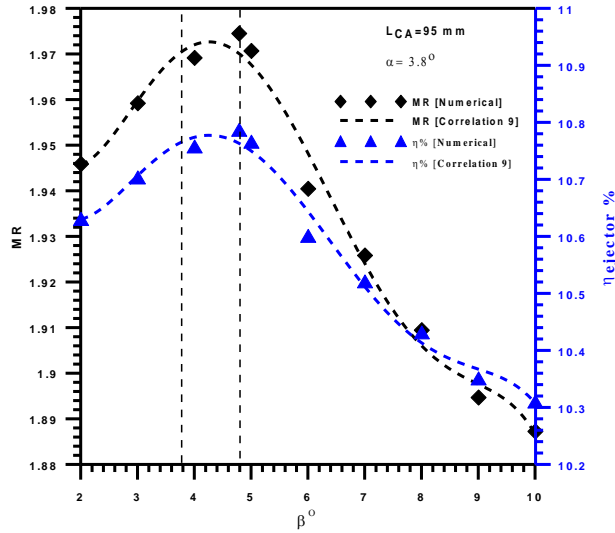


Fig. 4 Effect of constant-pressure mixing section half angle on mass ratio and ejector efficiency

Table 2. Coefficients of correlation (9) for $x=\beta$ and $Y=MR$ or η

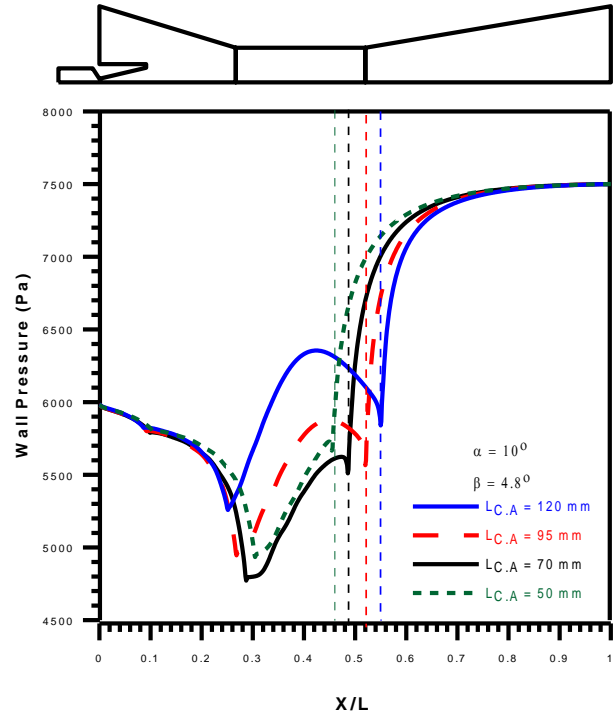
Y	MR	η
a_0	2.104998896	14.1679962
a_1	-0.2244428883	-4.850205352
a_2	0.1100710871	2.501127647
a_3	-0.02264035249	-0.6197396594
a_4	0.002036165661	0.0797232434
a_5	-6.702299232E-5	-0.005166207923
a_6	0.0	0.000133659926

Table 3. Coefficients of correlation (9) for $x=L_{CA}$ and $Y=MR$ or η

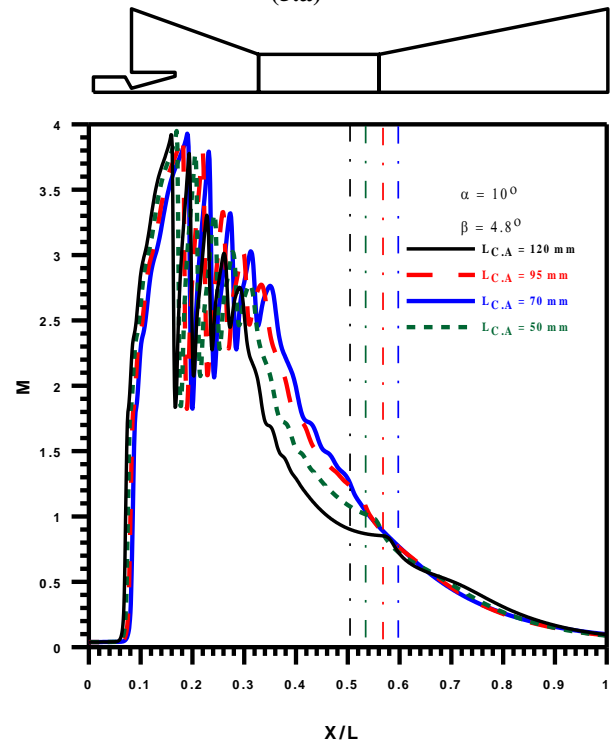
Y	MR	η
a_0	1.343920018	7.342301619
a_1	0.01713102664	0.09359274581
a_2	-0.0001619675085	-0.0008848847282
a_3	3.876859108E-7	2.118062721E-6

Comparisons between the numerically predicted ejector mass ratio and efficiency and the values obtained by the deduced correlations are illustrated respectively in Fig. 9. The comparisons show acceptable agreements where the minimum coefficients of determination of mass ratio and efficiency by correlation (9) were about 0.979 and 0.968 respectively. The numerical predictions of both ejector mass ratio and efficiency which are shown in Figs. 4, 6 and 8 are separately used to develop correlations relating ejector mass ratio and efficiency to constant-pressure mixing section half (β), constant-area mixing section length (L_{CA}) and

diffuser section half angle (α) while keeping all operating parameters as constants.



(5.a)



(5.b)

Fig. 5 Effect of constant-area mixing section length on wall static pressure and centerline Mach number distributions along the ejector axis

The obtained correlations for the steam ejector under consideration are in the following form:

$$Y = \sum_{k=0}^n a_k x^k \quad (9)$$

Where the different Coefficients, a_k are given in Tables (2, 3 and 4). The correlations are valid only for the ranges shown in Figs. 4, 6 and 8. Figure 10 depicts the contours of velocity streamline along the ejector axis. Severe separation is clearly seen starting from the beginning of the diffuser section which may be the reason of the decrease in efficiency shown in Fig. 8 at $\alpha = 10^\circ$.

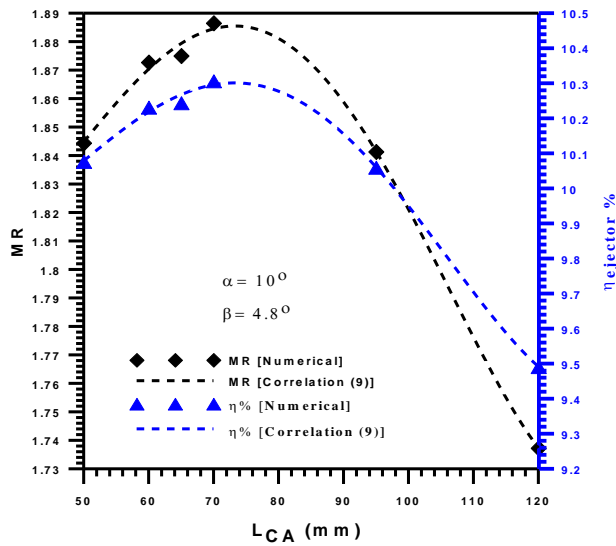


Fig. 6 Effect of constant-area mixing section length on mass ratio and ejector efficiency

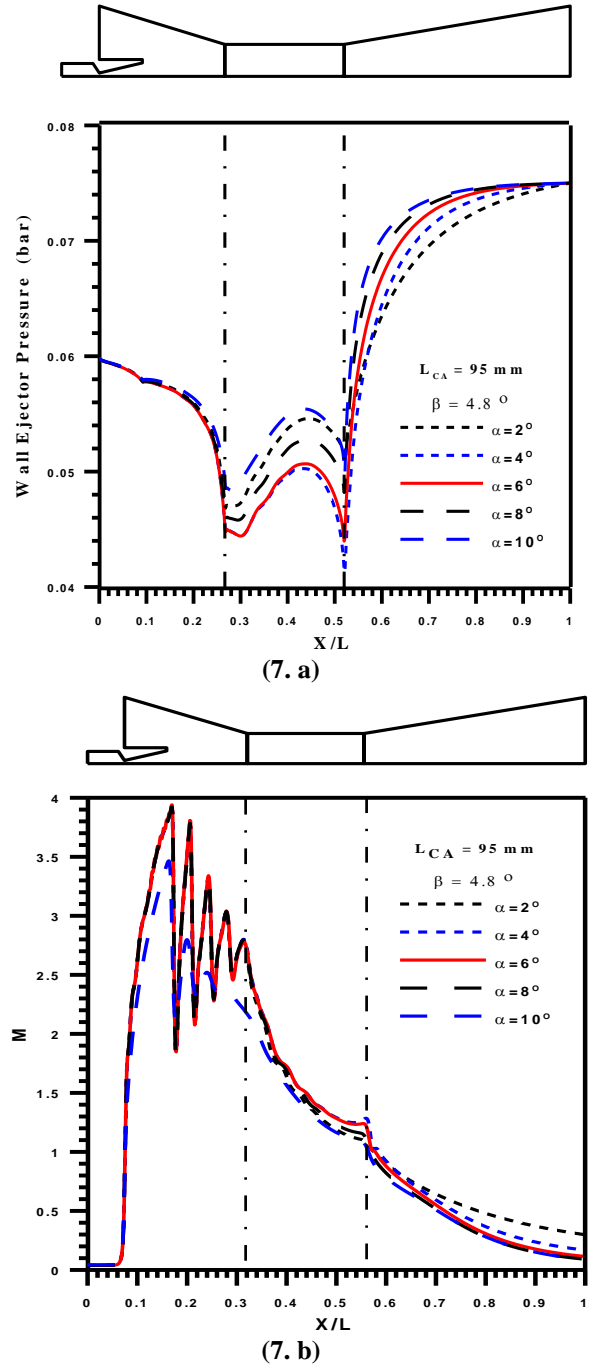


Fig. 7 Effect of diffuser section half angle on wall static pressure and centerline Mach number distributions along the ejector axis

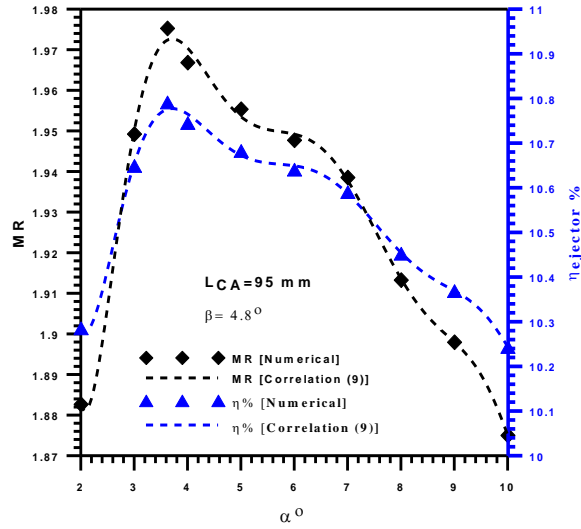
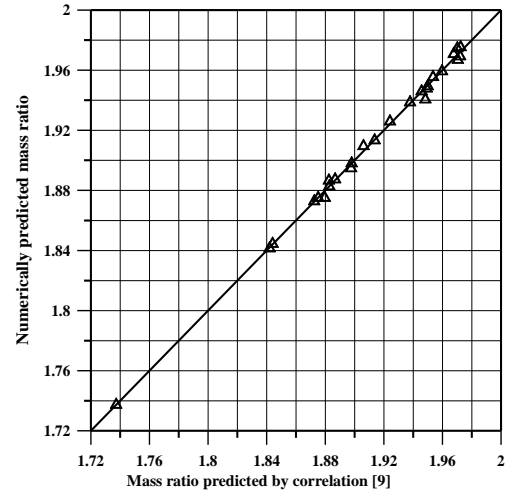


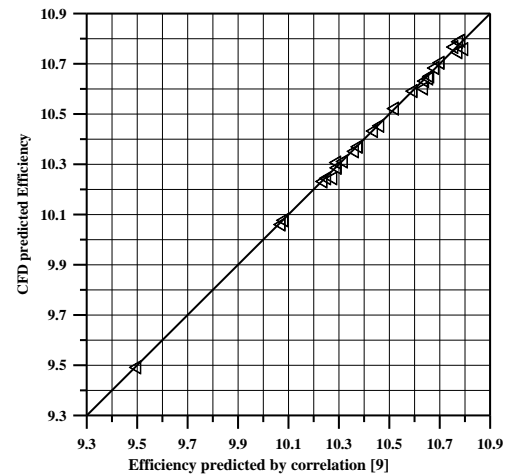
Fig. 8 Effect of diffuser section half angle on mass ratio and ejector efficiency

Table 4. Coefficients of correlation (9) for $x = \alpha$ and $Y = MR$ or η

Y	MR	η
a_0	8.213063853	44.8708191130485
a_1	-11.00818739	-60.141549359134
a_2	7.788715772	42.5524582312353
a_3	-2.944434984	-16.0864705233089
a_4	0.6582662992	3.59633731947124
a_5	-0.08987269131	-0.491005713248295
a_6	0.007363484058	0.0402292697505226
a_7	-0.0003326642623	-0.0018174603539619
a_8	6.370720235E-6	3.48054563313376E-5



(9. a)



(9. b)

Fig. 9 Comparison between numerically predicted mass ratio and efficiency and values predicted by correlation (9)

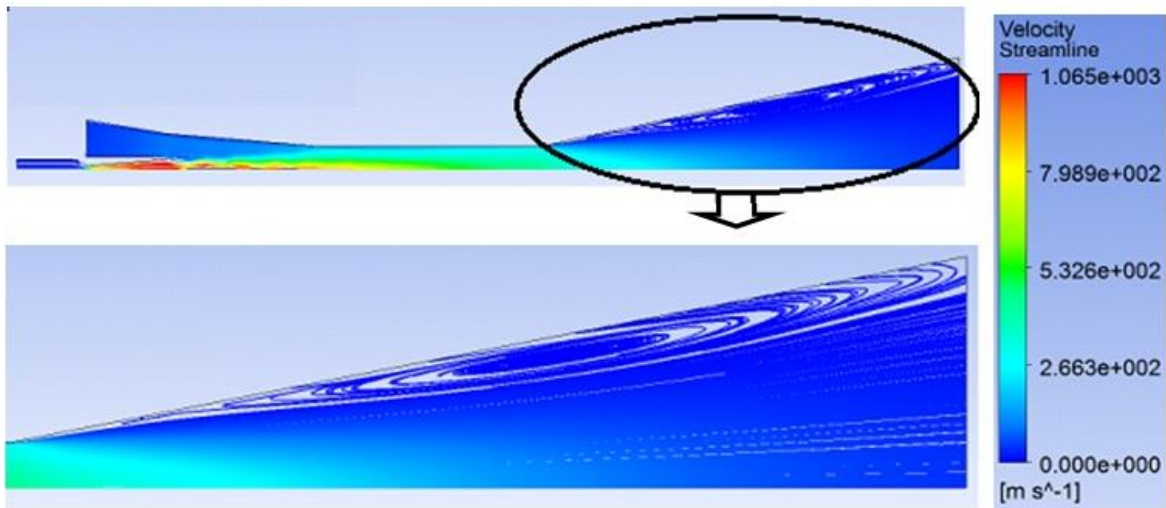


Fig. 10 Contours of velocity streamlines of steam ejector at $\beta=4.8^\circ$, $L_{CA}=70$ mm, and $\alpha=10^\circ$

5. Conclusions

The present paper introduces an optimization study for testing a steam ejector working at given operating conditions. Although an unrealistic single-phase ideal gas model was adapted, the proposed CFD model predicted well the mass flow ratio when validated against previously published experiments. The results led to concluding that, there are operational and geometrical constraints for using the steam ejectors in order to optimize their performances. For instance, it is important to determine the optimum angle of the diffuser at a given operating condition for optimum efficiency of the ejector. Otherwise, the un-optimized diffuser angle will consequently lead to smaller value of mass ratio.

Moreover, An optimum value of the ejector efficiency and mass ratio took place at about $\beta = 4.8^\circ$, $L_{CA} = 70$ mm and $\alpha = 3.6^\circ$ at given operating conditions which means that for every operating conditions range there is an optimum geometry that should be selected properly. Correlations for ejector optimum efficiency and mass ratio design were obtained by fitting the numerical results and relating these optimum values to three ejector geometric parameters, (β , L_{CA} and α).

Finally, the results provided appropriate guidance for ejector efficiency assessment and optimization to make ejectors more economically and technologically attractive in industrial applications. Additionally, the results concerning the pressure and Mach number distributions along the ejector axis led to better understanding of the mixing process in the ejector and the phenomenon of its operation which is essential for optimum ejector modeling. Future continuation of the present work will be conducted using a real steam model taking into consideration condensation process and shocks in comparison with the ideal steam model.

Nomenclatures

C_p specific heat capacity [J/kg.K]
 C_μ dimensionless constant of the turbulence model
 D diameter [m]
 h specific enthalpy of evaporation [J/kg]
 k turbulent kinetic energy [m^2/s^2]
 K thermal conductivity [W/m.K]
 L_{CA} constant-area mixing section length [m]
 \dot{m} mass flow rate [kg/s]
 MR mas ratio, \dot{m}_s/\dot{m}_m
 M_w molecular weight [kg/kmole]
 M Mach Number
 P pressure [Pa]
 u x -direction velocity [m/s]
 v r -direction velocity [m/s]

r radius, [m]
 T temperature [K]
 x, r cylindrical Coordinates
 α_{eff} effective thermal diffusivity
 α the diffuser section half angle
 β the convergent section half angle
 μ viscosity [kg/m.s]
 μ_t turbulent viscosity [kg/m.s]
 μ_{eff} effective dynamic viscosity [kg/m.s]
 ρ density [kg/m^3]
 ε turbulence dissipation rate [m^2/s^3]
 τ_{ij} shear stress [Pa]
 η the ejector efficiency
 η^* coefficient in equation (8)
 ω Specific turbulent dissipation rate (mean frequency of turbulence), $\omega = \varepsilon/k$ [1/s]
 G_k turbulent kinetic energy mean velocity gradients
 G_b buoyancy turbulence kinetic energy
 S_k, S_ε the user-defined source terms
 S_U, S_V x and r directions source terms
 S_h the energy source term
 S_{ij} the strain rate tensor
 \vec{V} the velocity vector [m/s]
 $C_1, C_2, C_{1\varepsilon}, C_{2\varepsilon}$ constants in equation (7)

Abbreviations

COP coefficient of performance
 REFPROP Reference properties

Subscripts

b back
 i, j describe the direction. When i or $j=1$, this case corresponding to the x -direction, i or $j=2$ means the r -direction.
 m motive
 s suction

References

- [1] Aphornratana S. Theoretical study of a steam ejector refrigerator. International Energy Journal 1996; 18: 61-73.
- [2] Sun D. Variable geometry ejectors and their applications in ejector refrigeration systems. Energy 1996; 21: 919-29.
- [3] Deberne N, Leone JF, Duque A, Lallemand A. A model for calculation of steam injector performance. International Journal of Multiphase Flow 1999; 25: 841-55.
- [4] Riffat SB, Omer SA. CFD modeling and experimental investigation of an ejector refrigeration system using methanol as the working fluid. International Journal of Energy Reservation 2001; 25:115-28.
- [5] Aphornratana S, Eames IW. A small capacity steam-ejector refrigerator: experimental

- investigation of a system using ejector with movable primary nozzle. *International Journal of Refrigeration* 1997; 20: 352–58.
- [6] Chunnanond K, Aphornratana S. An experimental investigation of a steam ejector refrigerator: the analysis of the pressure profile along the ejector. *Applied Thermal Engineering* 2004; 27: 311-22.
- [7] Rusly E, Aye L, Charters WS, Ooi A. CFD analysis of ejector in a combined ejector cooling system. *Int J Refrig* 2005; 28:1092-101
- [8] Yapıcı R and Ersoy HK. Performance characteristics of the ejector refrigeration system based on the constant area ejector flow model. *Energy Conversion and Management* 2005; 46: 3117-35.
- [9] Pianthong K, Sheehanam W, Behnia M, Sriveerakul T, Aphornratana S. Investigation and improvement of ejector refrigeration system using computational fluid dynamics technique. *Energy Convers Manage* 2007; 48: 2556-64
- [10] Hewedy NI, Hamed MH, Abou-Taleb FS, and Ghonim TA. Optimal performance and geometry of supersonic ejector. *ASME J. Fluids Eng.* 2008; 130: 041204.
- [11] Li HJ, Shen SQ. Effect of mixing chamber structure on a steam ejector performance. *The Fifth International Conference on Fluid Mechanics* 2007, Aug.15-19, Shanghai, China.
- [12] Sriveerakul T, Aphornratana S, Chunnanond K. Performance prediction of steam ejector using computational fluid dynamics: Part 1. Validation of the CFD results *International Journal of Thermal Sciences* 2007; 46: 812-22.
- [13] Sriveerakul T, Aphornratana S, Chunnanond K. Performance prediction of steam ejector using computational fluid dynamics: part 2. Flow structure of a steam ejector influenced by operating pressures and geometries. *Int. J. Therm. Sci.* 2007; 46: 823-33.
- [14] Varga S, Oliveira AC, Diaconu B. Influence of geometrical factors on steam ejector performance-A numerical assessment. *Int. J. Refrig.* 2009; 32: 1694-701.
- [15] Varga S, Oliveira AC, Diaconu B. Numerical assessment of steam ejector efficiencies using CFD. *Int. J. Refrig.* 2009; 32: 1203-211.
- [16] Zhang Qi, Jiepeng H, Ruofei L, Ruwu W. Numerical simulation and performance study of steam ejector using CFD. *Int. J. Advanced Science Letters* 2011; 4: 2276-80.
- [17] Ghonim TA. Two-phase flow (gas-liquid) through ejectors. A Ph.D thesis in Mech. Power Eng. Dept., Menofia University, 2014.
- [18] Wang L, Chen W, Hou W, Zhao H, Zhang H. Experimental investigation on ejector performance near critical back pressure. *International journal of refrigeration* 2017; 80: 158–68.
- [19] Huang Z, Zhao H, Yu Z, Han J. Simulation and optimization of a R744 twotemperature supermarket refrigeration system with an ejector. *International Journal of Refrigeration* 2018; 90: 73–82.
- [20] Chen J, Li Y, Chen W, Luo X, Ying C, Yang Z, Eames IW. Investigation of the ejector nozzle in refrigeration system. *Energy* 2018;157: 571-87.
- [21] Zhang H, Wang L, Jia L, Wang X. Assessment and prediction of component efficiencies in supersonic ejector with friction losses. *Applied Thermal Engineering* 2018;129: 618–27.
- [22] Zhang H, Wang L, Jia L, Zhao H, Wang C. Influence investigation of friction on supersonic ejector performance. *International journal of refrigeration* 2018; 85: 229–39.
- [23] Hongqiang W, Zhongliang L, Bing H, Yanxia L. Numerical investigation of the influences of mixing chamber geometries on steam ejector performance. *Desalination* 2014; 353: 15–20.
- [24] Ansys Fluent 16 theory's guide, 2014.
- [25] Farag MS. A numerical study for predicting steam ejector performance at different pressure ratios. *17th International Conference on Aerospace Sciences & Aviation Technology (ASAT 17)* 2017; April 11 – 13 – Military Technical College, Cairo, EGYPT.
- [26] Shih TH, Lou WW, Shabbir A, Yang Z, Zhou J. A new k–e eddy viscosity model for high Reynolds number turbulent flow-model development and validation. *Comput. Fluids* 1995; 24: 227-38.